Lipid droplets fuel SARS-CoV-2 replication and production of inflammatory mediators

Suelen da Silva Gomes Dias[1#], Vinicius Cardoso Soares[1,2#], André C. Ferreira[1,3,4], Carolina Q. Sacramento[1,3], Natalia Fintelman-Rodrigues[1,3], Jairo R. Temerozo[5,6], Lívia Teixeira[1], Ester Barreto[1], Mayara Mattos[1,3], Caroline S. de Freitas[1,3], Isaclaudia G. Azevedo-Quintanilha[1], Pedro Paulo A. Manso[7], Eugenio D. Hottz[1,8], Camila R. R. Pão[1], Dumith C. Bou-Habib[5,6], Fernando A. Bozza[9,10], Thiago M. L. Souza[1,3], Patrícia T. Bozza[1]*

 # - These authors contributed equally to this work

1- Laboratory of Immunopharmacology, Oswaldo Cruz Institute (FIOCRUZ), Rio de Janeiro, RJ, Brazil.

2- Program of Immunology and Inflammation, Federal University of Rio de Janeiro, UFRJ, Rio de Janeiro, RJ, Brazil.

3- National Institute for Science and Technology on Innovation on Diseases of Neglected Populations (INCT/IDNP), Center for Technological Development in Health (CDTS), FIOCRUZ, Rio de Janeiro, RJ, Brazil.

4- Universidade Iguaçu, Nova Iguaçu, RJ, Brazil.

5- Laboratory on Thymus Research, Oswaldo Cruz Institute (FIOCRUZ), Rio de Janeiro, RJ, Brazil.

6- National Institute for Science and Technology on Neuroimmunomodulation (INCT/NIM), Oswaldo Cruz Institute, Fiocruz, Rio de Janeiro, RJ, Brazil.

7- Laboratory of Patology, Oswaldo Cruz Institute (FIOCRUZ), Rio de Janeiro, RJ, Brazil.

8- Laboratory of Immunothrombosis, Department of Biochemistry, Federal University of Juiz de Fora (UFJF), Juiz de Fora, MG, Brazil;

9- National Institute of Infectology (INI), FIOCRUZ, Rio de Janeiro, Brazil.

10- D'Or Institute for Research and Education (IDOR), Rio de Janeiro, Brazil.

Keywords: SARS-CoV-2; COVID-19; Lipid metabolism; Lipid droplet; Pro-inflammatory cytokines.

*Corresponding author

Patrícia T. Bozza

pbozza@ioc.fiocruz.br or pbozza@gmail.com

Abstract

Viruses are obligate intracellular parasites that make use of the host metabolic machineries to meet their biosynthetic needs, identifying the host pathways essential for the virus replication may lead to potential targets for therapeutic intervention. The mechanisms and pathways explored by SARS-CoV-2 to support its replication within host cells are not fully known. Lipid droplets (LD) are organelles with major functions in lipid metabolism and energy homeostasis, and have multiple roles in infections and inflammation. Here we described that monocytes from COVID-19 patients have an increased LD accumulation compared to SARS-CoV-2 negative donors. *In vitro*, SARS-CoV-2 infection modulates pathways of lipid synthesis and uptake, including CD36, SREBP-1, PPARγ and DGAT-1 in monocytes and triggered LD formation in different human cells. LDs were found in close apposition with SARS-CoV-2 proteins and double-stranded (ds)-RNA in infected cells. Pharmacological modulation of LD formation by inhibition of DGAT-1 with A922500 significantly inhibited SARS-CoV-2 replication as well as reduced production of pro-inflammatory mediators. Taken together, we demonstrate the essential role of lipid metabolic reprograming and LD formation in SARS-CoV-2 replication and pathogenesis, opening new opportunities for therapeutic strategies to COVID-19.

Introduction

The coronavirus disease 2019 (COVID-19) caused by the novel severe acute respiratory syndrome-coronavirus 2 (SARS-CoV-2) has rapidly spread in a pandemic, representing an unprecedented health, social and economic threat worldwide (Lu et al., 2020; Wu et al., 2020). This newly emerged SARS-CoV-2 belongs to the *Betacoronavirus* genus of the subfamily *Orthocoronavirinae* in the *Coronaviridae* family. Like other Coronavirus, the SARS-CoV-2 is an enveloped non-segmented positive-sense RNA (+RNA) virus (Zhu et al., 2020), which genome sequence is similar to the already known SARS-CoV (Zhou et al., 2020b). Despite the similarity with other members of the *Betacoronavirus* genus, the pathogenesis of SARS-CoV-2 infection presents unique properties that contribute to its severity and pandemic-scale spread. Therefore, it is necessary to understand how the virus interacts and manipulate host cell metabolism to develop novel strategies to control the clinical progression of the infection and to limit the SARS-CoV-2 pandemic.

Viruses are obligated intracellular pathogens that require host cell machinery to replicate (Chazal and Gerlier, 2003; Novoa et al., 2005; Takahashi and Suzuki, 2011). Viruses interact with several intracellular structures and have the ability to reprogram the cellular metabolism to benefit viral replication (Abrantes et al., 2012; Syed et al., 2010; Zhang et al., 2017). Accumulated evidence points to major roles of lipid droplets (LD) for virus replication cycle and pathogenesis, highlighting the potential of these organelles as targets for drug development. Many studies have demonstrated the interaction of viral molecules with LD-related components, and the relevance of these organelles for viral replication as already demonstrated in several positive-strand RNA (+ RNA) viruses such as *Flaviviridae* members, rotavirus and reovirus (Cheung et al., 2010; Coffey et al., 2006; Filipe and McLauchlan, 2015; Lyn et al., 2013; Samsa et al., 2009; Villareal et al., 2015). Accordingly, pharmacological interventions that alter the synthesis of fatty acids, enzymes associated with lipid metabolism and the formation of LDs reduce viral replication and assembly (Herker et al., 2010; Martín-Acebes et al., 2011; Villareal et al., 2015; Yang et al., 2008; Zhang et al., 2017). In addition, LDs play an important role in the infection pathogenesis and inflammatory processes (Herker and Ott, 2012; Pereira-Dutra et al., 2019).

Here we demonstrate major effects of SARS-CoV-2 to modulate cellular lipid metabolism in human cells favoring increased de novo lipid synthesis and lipid remodeling, leading to increased LD accumulation in human cells. We also reported increased LD accumulation in monocytes from COVID-19 patients when compared to healthy volunteers. Importantly, the blockade of LD biogenesis with a pharmacological inhibitor of DGAT-1 decreased viral replication and pro-inflammatory cytokine production and prevented cell death. Collectively, our results uncover mechanisms of viral manipulation of host cell lipid metabolism to allow SARS-CoV-2 replication and may provide new insights for antiviral therapies.

Results

SARS-CoV-2 infection upregulates lipid metabolism, increasing LD biogenesis in human cells.

Viruses have the ability to modulate cellular metabolism with benefits for their own replication. Several +RNA viruses, including members of *Flaviviridae* family, as HCV (Boulant et al., 2007; Lyn et al., 2013) and DENV (Carvalho et al., 2012; Samsa et al., 2009), as well as reovirus (Coffey et al., 2006) and poliovirus (Viktorova et al., 2018) modify the lipid metabolism in different cells and trigger LD formation, using these host organelles at different steps of their replicative cycle.

Here, we demonstrated increased LD accumulation in human monocytes from COVID-19 patients when compared with healthy volunteers (Fig. 1A and B). Likewise, we demonstrated that in vitro infection with SARS-CoV-2 with a multiplicity of infection (MOI) of 0.01 triggers the increase of LDs in primary human monocytes within 24 hours (Fig. 1C and D), as well as in a human lung epithelial cell line (A549), and human lung microvascular endothelial cell line (HMVEC-L) after 48 hours post-infection (Supplementary Fig. 1).

Lipid metabolism alterations in cells and plasma are emerging as major phenotypes during COVID-19 and SARS-CoV-2 infection (Shen et al., 2020). To gain insights on the mechanisms involved in LD formation, we evaluated whether SARS-CoV-2 infection could modulate the expression of the proteins associated with lipid metabolism involved in lipid uptake and de novo lipid synthesis (Fig. 1E). As shown in figure 1E-G, SARS-CoV-2 infection of human primary monocytes up-regulated the pathways involved in lipid uptake such as CD36, the major transcriptional factors involved in lipogenesis, PPARγ and SREBP-1, and the enzyme DGAT-1, which is involved in triacylglycerol synthesis, after 24 hours of infection.

Altogether, these data suggest that SARS-CoV-2 is able to modulate multiple pathways of lipid metabolism and remodeling, including in immune cells from COVID-19 patients, culminating in new LD assembling in human cells.

Inhibition of LD formation decreases viral replication and prevents cell death in SARS-CoV-2 infected monocytes.

DGAT-1 is a key enzyme involved in the final step of triacylglycerol synthesis and thus is central to remodel and finish the biogenesis of LDs (Chitraju et al., 2017) .

123 During HCV infection, DGAT-1 was shown to be required for LD biogenesis, and to
124 control HCV protein trafficking to LDs (Camus et al., 2013). Consequently, DGAT-1
125 inhibition blocks HCV use of LDs as replication platforms and inhibits viral particle
126 formation (Camus et al., 2013; Herker et al., 2010). To assess the involvement of DGAT-
127 1 in LD biogenesis during the SARS-CoV-2 infection, we treated A549 cells with
128 A922500, an inhibitor of the enzyme DGAT-1, for 2 hours at different concentrations
129 prior to SARS-CoV-2 infection and evaluated the LD biogenesis 48 hours after infection.
130 As shown in figure 2A and B, treatment with A922500 inhibited in a dose dependent
131 manner the LD formation triggered by SARS-CoV-2 infection. Similarly, pre-treatment
132 with A922500 also blocked LD induced by SARS-CoV-2 in monocytes (Fig. 2A and C).
133 Human monocytes infected with SARS-CoV-2 were shown to sustain viral
134 genome replication, express higher levels of pro-inflammatory cytokines and may
135 undergo cell death (Codo et al., 2020). To gain insights on the functions of LDs in SARS-
136 CoV-2 infection, LD biogenesis was inhibited by A922500, a DGAT-1 inhibitor.
137 Treatment with A922500 significantly reduced the viral load in human primary
138 monocytes (Fig. 3A), suggesting a role for DGAT-1 and LD in SARS-CoV-2 replication.
139 It has already been demonstrated the capacity of the SARS-CoV-2 infection to
140 induce cell death in monocytes, as evidenced by the leak of LDH to the extracellular space
141 (Fintelman-Rodrigues et al., 2020). Cell death after viral infections can occur due to
142 changes in cellular homeostasis caused by the virus replication per se and/or by the
143 heightened inflammatory response. Here, we measured the death of human primary
144 monocytes infected with SARS-CoV-2 by the release of LDH into the supernatant, and
145 also by the analysis of cell morphology observed in phase contrast. Our data show that
146 SARS-CoV-2 triggered increased LDH release in the supernatant and that infected cells
147 exhibited morphologic alterations with membrane rupture/damage compatible with
148 necrosis (Fig. 3B and C). Similar to the observed for viral replication, DGAT-1 and LD
149 inhibition with 10 μM of A922500 was able to inhibit SARS-CoV-2-induced cell death
150 (Fig. 3B and C).

151 **Lipid droplets are involved in SARS-CoV-2 heightened inflammatory response**

152 Dysregulated immune response, with increased pro-inflammatory
153 cytokine/chemokine production is observed during severe COVID-19 and associates with
154 the outcome of the disease (Coperchini et al., 2020). We observed that primary human
155 monocytes infected with SARS-CoV-2 exhibit increased production of leukotrienes

156 (LTB$_4$ and cysLT), pro-inflammatory cytokines (IL-6, TNFα and IL-12) and chemokines
157 (IL-8 and CXCL10) in comparison with uninfected cells (Fig. 3D, E and F). Regarding
158 anti-inflammatory mediators, SARS-CoV-2 infection increased IL-10 and reduced IL-4
159 production in comparison with uninfected monocytes (Fig. 3G).

160 LDs are organelles with major functions in inflammatory mediator production and
161 innate signaling in immune cells. To evaluate if LDs contribute to SARS-CoV-2-induced
162 inflammation, monocytes were pre-treated with A922500, the secreted levels of lipid
163 mediators, cytokine and chemokines were measured 24 h after infection. It has been well
164 established that LDs are organelles that compartmentalize the eicosanoid synthesis
165 machinery and are sites for eicosanoid formation (Bozza et al., 2011). Here, we
166 demonstrated that SARS-CoV-2 infection increased LTB$_4$ and cysLT production in
167 comparison with uninfected monocytes (Fig 3D). The pretreatment with DGAT-1
168 inhibitor A922500 reduced the synthesis of both lipid mediators by infected cells (Fig.
169 3D). These data point out the importance of LD for the production of these pro-
170 inflammatory lipid mediators. We also observed that A922500 treatment downregulated
171 the chemokines IL-8 and CXCL10, and the pro-inflammatory cytokines IL-6, TNFα and
172 IL-12 (Fig. 3E and F), without affecting the anti-inflammatory cytokine IL-10 (Fig. 3G).
173 In addition to lowering the pro-inflammatory mediators, inhibition of LDs may shift the
174 inflammatory profile by increasing the anti-inflammatory cytokine IL-4 (Fig. 3G).

175 Altogether, our data indicate that LDs have important functions in the modulation
176 of inflammatory mediators production in SARS-CoV-2-infected monocytes and suggest
177 that LD inhibition may reduce the exaggerated inflammatory process caused by the
178 cytokine storm.

179 **Lipid droplets are sites for SARS-CoV-2 replication.**

180 The up regulation of the lipid metabolism and LD biogenesis by the new SARS-
181 CoV-2 suggest that the virus may explore host metabolism to favor it is replication using
182 the LDs as a replication platform, as demonstrated for HCV (Boulant et al., 2007; Camus
183 et al., 2013; Lee et al., 2019) and DENV (Samsa et al., 2009). To evaluate this, we used
184 a VERO E6 cell line that has a highly replicative capacity.

185 For these experiments, we pre-treated the VERO cells with a range of
186 concentrations of DGAT-1 inhibitor A922500 (0.1 - 50 μM) for 2 hours, followed by
187 infection with SARS-CoV-2 (MOI 0.01) for 24 hours. The supernatant was used to

188 perform a plaque assay. Here, we observed that A922500 significantly inhibited SARS-
189 CoV-2 replication in a dose dependent manner with an IC50 of 3.78 µM (Fig. 4A and B).
190 To gain insights on the interaction of the SARS-CoV-2 with LDs we labeled the
191 virus using immune serum from a convalescent COVID-19 patient that exhibit high anti-
192 SARS-CoV-2 titers. For that, we stained the LDs using a BODIPY probe and analyzed
193 the co-localization between the viral proteins and LDs by confocal microscopy. As shown
194 in figure 4C, intense immunoreactivity (red) was obtained in SARS-CoV-2 infected cells,
195 whereas no labeling was observed in uninfected cells, indicative of specific SARS-CoV-
196 2 labeling with COVID-19 convalescent serum (Fig. 4C). As observed for monocytes and
197 lung cells, Vero E6 infected cells increased LD biogenesis (green). Then, we examined
198 the spatial relationship between SARS-CoV-2 and LDs. Confocal analysis showed a close
199 apposition of SARS-CoV-2 immunoreactivity with BODIPY-labeled LDs (red arrows)
200 and also co-localization of viral protein(s) with BODIPY-labeled LDs (yellow; fuchsia
201 arrows) in the infected cells (Fig. 4C-D).
202 Accumulating evidence indicate that host LDs play an important role in virus
203 replicative cycle, including as hubs for viral genome replication and viral particle
204 assembling (Laufman et al., 2019; Lee et al., 2019; Miyanari et al., 2007; Samsa et al.,
205 2009) . To assess if LDs are associated with SARS-CoV-2 replication, we use a specific
206 antibody for double stranded (ds)-RNA (J2 clone). As shown in figure 4E, we observed
207 strong labeling of the ds-RNA in cells infected with the SARS-CoV-2 compared to
208 uninfected cells. Similar to labeling detected with convalescent COVID-19 polyclonal
209 serum, we observed close apposition and/or co-localization between BODIPY-labeled
210 LDs and ds-RNA (Fig. 4E and E`).
211 Collectively, our data suggest that SARS-CoV-2 uses LDs as a replication
212 platform, and establish that pharmacological targeting of LD formation inhibit SARS-
213 CoV-2 replication, emerging as a potential strategy for antiviral development.
214

Discussion

Most positive-strand RNA virus are able to modulate the host lipid metabolism and to highjack LDs to enhance their fitness and replication/particle assembling capacity (Herker and Ott, 2012; Pereira-Dutra et al., 2019). The pathways and mechanisms used may vary according to the virus and the host cell infected. The mechanisms and pathways explored by SARS-CoV-2 to support its replication within host cells are still largely unknown. Here we provide evidence that LDs participate at two levels of host pathogen interaction in SARS-CoV-2 infection: first, they are important players for virus replication; and second, they are central cell organelles in the amplification of inflammatory mediator production. First, we demonstrated that SARS-CoV-2 modulates pathways of lipid uptake and lipogenesis leading to increased LD accumulation in human host cells. We further showed that LDs are in close proximity with SARS-CoV-2 proteins and replicating genome, a finding suggestive that LDs are recruited as part of replication compartment. Second, we showed that inhibition of DGAT-1 blocked LD biogenesis, and reduced virus replication, cell-death and pro-inflammatory mediator production.

LD biogenesis is a multi-mediated and highly coordinated cellular process that requires new lipid synthesis and/or lipid uptake and remodeling, but the molecular mechanisms involved in LD formation during inflammation and infection are still not completely understood. Here, we showed the increased expression of SREBP-1 and the nuclear receptor PPARγ after SARS-CoV-2 infection indicative of reprogramming of cells towards a lipogenic phenotype. Accordingly, increased expression of SREBP-1 has been reported after respiratory viruses including MERS-CoV, SARS-CoV, and shown to regulate the increase of the LD and the accumulation of the cholesterol during the infection (Yuan et al., 2019). Consistently, targeting the SREBP-associated lipid biosynthetic pathways were shown to have antiviral properties (Yuan et al., 2019). The transcription factor PPARγ is activated by lipid ligands and promotes the expression of proteins involved in lipid homeostasis and LD biogenesis, and has been implicated in infectious and non-infectious LD biogenesis in monocytes/macrophages (Almeida et al., 2014; Souza-Moreira et al., 2019). Based on these data we can suggest that these two transcription factors are critical for SARS-CoV-2 infection, favoring the lipid synthesis and LD formation. One important gene up regulated by PPARγ is the membrane receptor CD36 (Cheng et al., 2016). CD36 plays an important role in the transport and uptake of long-chain fatty acids into cells and participates in pathological processes, such as

248 metabolic disorders and infections (Febbraio et al., 2001). Previous reports showed that
249 CD36 levels are increased in HCV and HIV-1 infections (Berre et al., 2013; Meroni et
250 al., 2005) and that it facilitates the viral attachment on host cell membrane contributing
251 to viral replication (Cheng et al., 2016). Our results demonstrated that SARS-CoV-2
252 infection increase the CD36 expression in monocytes, suggesting the increase of lipids
253 uptake can contribute to LD formation, observed after the infection.

254 Numerous studies established LDs as key organelles during +RNA viruses
255 replicative cycle (Herker and Ott, 2012). Here, we observed strong labeling of the SARS-
256 CoV-2 proteins and ds-RNA intimately associated to the LD and in some cases
257 colocalizing with LD. This fact highly suggests that SARS-CoV-2 recruits LDs to
258 replication compartments and could use them as building blocks to fuel its own
259 replication. Indeed, recent studies have shed light on active mechanisms of LD
260 recruitment to viral replication compartments with bi-directional content exchange and
261 essential functions to replication and virus particle assembly (Laufman et al., 2019; Lee
262 et al., 2019).

263 DGAT-1, the key enzyme for triacylglycerol synthesis, is critical for LD
264 biogenesis and mediate viral protein trafficking to LD by HCV and other viruses.
265 Moreover, pharmacological suppression of DGAT1 activity inhibits HCV replication at
266 the assembly step (Camus et al., 2013; Herker et al., 2010). We observed that DGAT-1
267 expression increases after SARS-CoV-2 infection and that this enzyme can contribute for
268 the LD remodeling in the host cells. Pharmacological inhibitors of lipid metabolism
269 protein are able to modulate the LD formation. Therefore, we used the DGAT-1 inhibitor
270 (A22500) during SARS-CoV-2 infection and observed that this treatment reduced the LD
271 biogenesis in monocytes and A549 cells, as well as decrease the viral load of SARS-CoV-
272 2 in monocytes. Importantly, pharmacologically suppressing DGAT1 activity dose
273 dependently inhibited SARS-CoV-2 infectious particle formation in VERO E6 cells with
274 an IC50 of 3.78 μM. Thus, suggesting that DGAT-1 activity and LD formation are crucial
275 to SARS-CoV-2 replication and assembly in these cells.

276 Dysregulated monocyte responses are pivotal in the uncontrolled production of
277 cytokines during the infection with respiratory viruses, such as influenza A virus (Gao et
278 al., 2013; Peschke et al., 1993). Dysregulated immune response with key involvement of
279 monocytes, and increased pro-inflammatory cytokine/chemokine production is also
280 observed during severe COVID-19 and is associated with the outcome of the disease
281 (Coperchini et al., 2020; Zhou et al., 2020a). SARS-CoV-2 infection of human monocytes

282 in vitro recapitulate most of the pattern of inflammatory mediator production associated
283 with COVID-19 severity, including the enhancement of the IL-6 and TNFα levels, and
284 the consistent cell death, measured by LDH release (Fintelman-Rodrigues et al., 2020;
285 Temerozo et al., 2020; Zhou et al., 2020a). We showed that SARS-CoV-2 infection
286 generated a large amount of inflammatory lipid mediators, and cytokine synthesis by
287 monocytes. Blockage of DGAT-1 activity lead to inhibition of the LDs and significantly
288 reduced leukotriene production and pro-inflammatory cytokines released by monocytes,
289 suggesting an important role for LDs to control the inflammatory process, and
290 consequently to prevent the cell death-related with the uncontrolled inflammation. This
291 finding is in agreement with the well-established role of LDs in inflammation and innate
292 immunity (Bozza and Viola, 2010; Pereira-Dutra et al., 2019). Therefore, our data support
293 a role for LD in the heightened inflammatory production triggered by SARS-CoV-2 and
294 conversely, inhibition of LD biogenesis by targeting DGAT1 activity may have beneficial
295 effects on disease pathogenesis.

296 In summary, our data demonstrate that SARS-CoV-2 triggers reprograming of
297 lipid metabolism in monocytes and other cells leading to accumulation of LDs favoring
298 virus replication. The inhibition of LD biogenesis modulates the viral replication and the
299 pro-inflammatory mediator production. Therefore, our data support the hypothesis that
300 SARS-CoV-2 infection increases the expression of the lipid metabolism-related proteins
301 for their own benefit towards replication and fitness. Although, further studies are
302 certainly necessary to better characterize the full mechanisms and importance of the LDs
303 during the SARS-CoV-2 infection, our findings support major roles for LDs in SARS-
304 CoV-2 replicative cycle and immune response. Moreover, the finding that the host lipid
305 metabolism and LDs are required for SARS-CoV-2 replication suggests a potential
306 strategy to interfere with SARS-CoV-2 replication by blocking the DGAT1 and other
307 lipid metabolic pathway enzymes.

308

Acknowledgments

We thank the Hemotherapy Service from Hospital Clementino Fraga Filho (Federal University of Rio de Janeiro, Brazil) for providing buffy-coats. The authors thank the confocal imaging facility from the Rede de Plataformas Tecnológicas FIOCRUZ and Dr. Carmen Beatriz Wagner Giacoia Gripp for assessments related to BSL3 facility. This work was supported by grants from Inova program Fiocruz, Fundação de Amparo à Pesquisa do Estado do Rio de Janeiro (FAPERJ), Conselho Nacional de Desenvolvimento Científico e Tecnológico (CNPq) and Coordenação de Aperfeiçoamento de Pessoal de Nível Superior (CAPES) granted for Patrícia T. Bozza, Thiago Moreno L. Souza, Dumith Chequer Bou-Habib and Fernando A. Bozza.

Author Contribution.

Conceived the study: SSGD, VCS, FAB, TMLS, PTB; Designed the experiments: SSGD, VCS, TMLS; PTB; Performed the experiments: SSGD, VCS, ACF, CQS, NFR, JRT, LT, EB, MM, CSF, IGAQ, PPM, EH, CRRP; Analyzed the data: SSGD, VCS, DCBH, TMLS, PTB; Wrote the paper: SSGD, VCS, TMLS, PTB. All authors reviewed and approved the manuscript.

The authors declare no competing financial interests.

328 **Methodology**

329 **Cells, virus and reagents.** Blood were obtained from RT-PCR-confirmed COVID-19
330 patients and SARS-CoV-2-negative health volunteers. Human monocytes were isolated
331 from peripheral blood mononuclear cells (PBMCs) using density gradient centrifugation
332 (Ficoll-Paque, GE Healthcare). The PBMC were resuspended in PBS containing 1 mM
333 EDTA and 2 % fetal bovine serum (FBS; GIBCO) to the concentration of 10^8 cells/mL.
334 The cells were incubated with anti-CD14 antibodies (1:10) for 10 min and magnetic
335 beads-conjugates (1:20) for additional 10 min, followed by magnetic recovery of
336 monocytes for 5 min. Recovered monocytes were resuspended in PBS containing 1 mM
337 EDTA and 2 % FBS and subjected to two more rounds of selection in the magnet
338 according to the manufacturer's instructions (Human CD14+ selection kit, Easy Sep;
339 StemCell). The purity of monocyte preparations (>98% CD14+ cells) was confirmed
340 through flow cytometry.

341 Human primary monocyte was obtained through plastic adherence of PBMCs. Briefly,
342 PBMCs were isolated by Ficoll-Paque from peripheral blood or from buff-coat
343 preparations of healthy donors. PBMCs (2×10^6) were plated onto 48-well plates in low
344 glucose Dulbecco's modified Eagle's medium (DMEM; GIBCO). After 2 hours of the
345 plaque, non-adherent cells were washed out and the remaining monocytes were
346 maintained for 24 hours in DMEM containing 5% inactivated male human AB serum
347 (HS; Merck) and 100 U/mL penicillin-streptomycin (P/S; GIBCO) at 37 °C in 5 % CO_2.
348 The purity of human monocytes was above 90 %, as analyzed by flow cytometry analysis
349 (FACScan; Becton Dickinson) using anti-CD3 (BD Biosciences) and anti-CD16
350 (Southern Biotech) monoclonal antibodies.

351 Human lung epithelial carcinoma cell line (A549 - ATCC/CCL-185) and African green
352 monkey kidney (Vero subtype E6) were cultured in high glucose DMEM supplemented
353 with 10% FBS and 100 U/mL P/S, and were incubated at 37 °C in 5 % CO_2.

354 Human lung microvascular endothelial cell line (HMVEC-L - LONZA/CC-2527) was
355 maintained following the manufacturer's instructions. The cells were cultured in
356 endothelial growth medium (EGM™-2MV BulletKit™, Clonetics) supplemented with 5
357 % fetal bovine serum (FBS, Clonetics) and cells were incubated at 37 °C and 5 % CO_2.

358 SARS-CoV-2 was originally isolated from nasopharyngeal swabs of confirmed case from
359 Rio de Janeiro/Brazil (GenBank accession no. MT710714). The virus was amplified in
360 Vero E6 cells in high glucose DMEM supplemented with 2% FBS, incubated at 37°C in
361 5% CO_2 during 2 to 4 days of infection. Virus titers were performed by the tissue culture
362 infectious dose at 50% ($TCID_{50}$/mL) and the virus stocks kept in -80 °C freezers.
363 According to WHO guidelines, all procedures involving virus culture were performed in
364 biosafety level 3 (BSL3) multiuser facility.

365 **Infections and virus titration.** After 24h of cell plating, the SARS-CoV-2 infections
366 were performed at MOI of 0.01 in all cells with or without pre-treatment with the
367 pharmacological inhibitor of DGAT-1 (A922500 – Sigma CAS 959122-11-3) for two
368 hours. The Plaque-forming Assay was performed for virus titration in VERO E6 cells
369 seeded in 24-well plates. Cell monolayers were infected with different dilutions of the
370 supernatant containing the virus for 1h at 37°C. The cells were overlaid with high glucose
371 DMEM containing 2% FBS and 2.4% carboxymethylcellulose. After 3 days, the cells
372 were fixed with 10% formaldehyde in PBS for 3h. The cell monolayers were stained with
373 0.04% crystal violet in 20% ethanol for 1h. The viral titer was calculated from the count
374 of plaques formed in the wells corresponding to each dilution and expressed as plaque
375 forming unit per mL (PFU/mL).
376

377 **Lipid droplet staining.** Human primary monocytes, A549 cell line, and HMVEC cell
378 line were seeded in coverslips. The cells infected or not were fixed using 3.7%
379 formaldehyde. In addition, after isolation, the monocytes from COVID-19 patients were
380 fixed using 3.7% formaldehyde and adhered in coverslips through cytospin (500 x g for
381 5 min). The LDs were stained with 0.3% Oil Red O (diluted in 60% isopropanol) for
382 2 min at room temperature. The coverslips were mounted in slides using an antifade
383 mounting medium (VECTASHIELD®). Nuclear recognition was based on DAPI staining
384 (1 µg/mL) for 5 min. Fluorescence was analyzed by fluorescence microscopy with an
385 100x objective lens (Olympus, Tokyo, Japan). The numbers of LDs were automatically
386 quantified by ImageJ software analysis from 15 aleatory fields.
387

388 **Immunofluorescence staining.** VERO E6 cells were seeded in coverslips and after 48h
389 were fixed using 3.7% formaldehyde. Cells were rinsed three times with PBS containing
390 0.1 M CaCl2 and 1 M MgCl2 (PBS/CM) and then permeabilized with 0.1% Triton X-100

391 plus 0.2% BSA in PBS/CM for 10 min (PBS/CM/TB). Cells were stained with
392 convalescent serum from a patient to identify with COVID-19 at 1:500 dilution for
393 overnight, followed by a human anti-IgG-Alexa 546 at 1:1000 dilution for 1 h. The
394 double-RNA was labeling by mouse monoclonal antibody J2 clone - Scicons (Schönborn
395 et al., 1991) at 1:500 dilution for overnight, followed by a mouse anti-IgG-Dylight 550
396 at 1:1000 dilution for 1h. LDs were stained with BODIPY493/503 dye (dilution 1:5000
397 in water) for 5 min. The coverslips were mounted in slides using an antifade mounting
398 medium (VECTASHIELD®). Nuclear recognition was based on DAPI staining
399 (1 µg/mL) for 5 min. Fluorescence was analyzed by fluorescence microscopy with an
400 100x objective lens (Olympus, Tokyo, Japan) or Confocal Microscopy (Laser scanning
401 microscopy LSM710 Meta, Zeiss).

402 **SDS-PAGE and Western blot.** After 24h of SARS-CoV-2 infection, monocytes were
403 harvested using ice-cold lysis buffer (1% Triton X-100, 2% SDS, 150 mM NaCl, 10 mM
404 HEPES, 2 mM EDTA containing protease inhibitor cocktail - Roche). Cell lysates were
405 heated at 100 °C for 5 min in the presence of Laemmli buffer (20% β-mercaptoethanol;
406 370 mM Tris base; 160 µM bromophenol blue; 6% glycerol; 16% SDS; pH 6.8).
407 Twenty µg of protein/sample were resolved by electrophoresis on SDS-containing 10%
408 polyacrylamide gel (SDS-PAGE). After electrophoresis, the separated proteins were
409 transferred to nitrocellulose membranes and incubated in blocking buffer (5% nonfat
410 milk, 50 mM Tris-HCl, 150 mM NaCl, and 0.1% Tween 20). Membranes were probed
411 overnight with the following antibodies: anti-PPARγ (Santa Cruz Biotechnology, #SC-
412 7196 - H100), anti-CD36 (Proteintech-18836-1-AP), anti-SREBP-1 (Ab-28481), anti-
413 DGAT-1 (Santa Cruz Biotechnology, #SC-271934) and anti-β-actin (Sigma, #A1978).
414 After the washing steps, they were incubated with IRDye - LICOR or HRP-conjugated
415 secondary antibodies. All antibodies were diluted in blocking buffer. The detections were
416 performed by Supersignal Chemiluminescence (GE Healthcare) or by fluorescence
417 imaging using the Odyssey system. The densitometries were analyzed using the Image
418 Studio Lite Ver 5.2 software.

419 **Measurement of viral RNA load.** Supernatants from monocytes were harvested after
420 24h of SARS-CoV-2 infection and the viral RNA quantified through RT-PCR. According
421 to manufacter's protocols, the total RNA from each sample was extracted using QIAamp
422 Viral RNA (Qiagen®). Quantitative RT-PCR was performed using QuantiTect Probe RT-
423 PCR Kit (Quiagen®) in a StepOne™ Real-Time PCR System (Thermo Fisher Scientific).

424 Amplifications were carried out containing 2× reaction mix buffer, 50 µM of each primer,
425 10 µM of probe, and 5 µL of RNA template in 15 µL reaction mixtures. Primers, probes,
426 and cycling conditions recommended by the Centers for Disease Control and Prevention
427 (CDC) protocol were used to detect the SARS-CoV-2 (CDC, 2020). For virus
428 quantification it was employed the standard curve method. Cells of each sample were
429 counted before the PCR analyses for normalization. The Ct values for this target were
430 compared to those obtained to different cell amounts, 10^7 to 10^2, for calibration.

431 **Measurements of inflammatory mediators and LDH activity.** The monocyte
432 supernatant was obtained after 24 hours of SARS-CoV-2 infection with or without pre-
433 treatment with A922500 (10 µM). Cytokines and chemokines were measured in the
434 supernatant by ELISA following the manufacturer's instructions (Duo set, R&D). LTB_4
435 and cysLT were measured in the supernatant by EIA following the manufacturer's
436 instructions (Cayman Chemicals). Cell death was determined according to the activity of
437 lactate dehydrogenase (LDH) in the culture supernatants using a CytoTox® Kit according
438 to the manufacturer's instructions (Promega, USA).

439 **Ethics statement.** Experimental procedures involving human cells from healthy donors
440 were performed with samples obtained after written informed consent and were approved
441 by the Institutional Review Board (IRB) of the Oswaldo Cruz Foundation/Fiocruz (Rio
442 de Janeiro, RJ, Brazil) under the number 397-07. Experimental procedures involving
443 human patient cells were performed with samples obtained after written informed consent
444 from all participants or patients' representatives according to the study protocol approved
445 by the National Review Board (CONEP 30650420.4.1001.0008).

446 **Statistical analysis.** Data are expressed as mean ± standard error of the mean (SEM) at
447 least of three and maximum of five independent healthy donors. The paired two-tailed *t*-
448 test was used to evaluate the significance of the two groups. Multiple comparisons among
449 three or more groups were performed by one-way ANOVA followed by Tukey's multiple
450 comparison test. p values < 0.05 were considered statistically significant when compared
451 SARS-CoV-2 infection to the uninfected control (*) group or SARS-CoV-2 infection
452 with A922500 treat group (#).

453 **Figure Legends**

454 **Fig 1. SARS-CoV-2 infection modulates the lipid metabolism in human monocytes.**

455 (A and C) LDs were captured by fluorescent microscopy after Oil Red O staining (Red)
456 and nuclei stained with DAPI (Blue). (A) Representative images of monocytes from
457 COVID-19 patients and health volunteers. (C) Representative images of human
458 monocytes obtained from PBMC infected by SARS-CoV-2 with MOI of 0.01 for 24
459 hours. Scale bar 20µm. (B and D) LDs were evaluated by ImageJ software analysis by
460 the measurement of the fluorescent area. (E) Representative scheme of the increase of
461 proteins associated with lipid metabolism by SARS-CoV-2 infection in monocyte can
462 regulate the lipid droplet formation. (F) Monocytes were infected by SARS-CoV-2 with
463 MOI of 0.01 during 24h. Cell lysates were collected for the detection of CD36, PPAR-γ,
464 SREBP-1, DGAT-1 by Western blotting. β-actin level were used for control of protein
465 loading. (G) Densitometry data set of each protein. Data are expressed as mean ± SEM
466 of five healthy volunteers (HV) for ex vivo experiments and three healthy donors for LDs
467 staining and western blot. *$p < 0.05$ versus health volunteers or uninfected cells.

468 **Fig 2. The A922500 inhibits lipid droplet biogenesis induced by SARS-CoV-2 in**
469 **human pulmonary cells and monocytes.**

470 Human pulmonary cell (A549 cell line) and monocytes were pre-treated with DGAT-1
471 inhibitor A922500 for 2 hours before the infection with SARS-CoV-2 at MOI of 0.01
472 during 24h in monocytes and 48h in A549 cell line. (A) LDs were captured by fluorescent
473 microscopy after Oil Red O staining (Red) and nuclei stained with DAPI (Blue). Scale
474 bar 20µm. (B and C) LDs were evaluated by ImageJ software analysis by the
475 measurement of the fluorescent area of (B) A549 pre-treated with A922500 using
476 different concentrations (0.1, 1 and 10µM) and (C) LDs from monocytes pre-treated with
477 A922500 (10µM). Data are expressed as mean ± SEM obtained in four independent
478 experiments or donors. *$p < 0.05$ *versus* uninfected cells and #$p < 0.05$ *versus* A922500
479 treated cells.

480 **Fig 3. Inhibitor A922500 decreases the pro-inflammatory profile and cell death**
481 **induced by SARS-CoV-2 infection and reduces the viral load in human monocyte.**

482 Monocytes were pre-treated with DGAT-1 inhibitor A922500 (10µM) for 2 hours before
483 the infection with SARS-CoV-2 with MOI of 0.01 during 24h. (A) Cell death was
484 measured in the supernatant by LDH activity fold change in relation to the uninfected
485 cell. (B) Viral load by qPCR. Monocytes of each sample were counted for normalization.
486 (C) Images of phase contrast from monocytes. Scale bar 20µm. (D-G) The inflammatory
487 cytokines were measured in supernatants by ELISA (D) leukotrienes: CysLT and LTB_4,
488 (E) chemokines: IL-8 and CXCL-10, (F) pro-inflammatory: IL-6, TNF-α and IL-12 and
489 (G) anti-inflammatory cytokines: IL-10 and IL-4. Data are expressed as mean ± SEM
490 obtained in four independent donors. * $p < 0.05$ *versus* uninfected cells and #$p < 0.05$
491 *versus* A922500 treated cells.

492 **Fig 4. Lipid droplets is necessary for SARS-CoV-2 replication in VERO E6.**

493 VERO E6 were pre-treated with DGAT-1 inhibitor A922500 with different
494 concentrations (0.1, 1, 10 and 50µM) for 2 hours before the infection with SARS-CoV-2
495 with MOI of 0.01 for 24h. (A) Viral replication was determinate by Plaque assay. (B)
496 Representative Plaque assay. (C-E) Immunofluorescence analyses of VERO E6 after
497 SARS-CoV-2 infection with MOI of 0.01 for 48h. (C) The virus was detected by indirect
498 immunofluorescence using convalescent donor serum (Red or white) or (E) the double
499 strain RNA was detected by indirect immunofluorescence by J2 antibody (Red), the lipid
500 droplets were stained with BODIPY 493/503 (Green) and nuclei stained with DAPI
501 (Blue). (C' and E') Representative zoom images. Data are expressed of four independent
502 experiments for SARS-CoV-2 replication and three for immunofluorescent analyse. #p
503 <0.05 versus A922500 treated cells. Scale bar 20µm.

504 **Fig S1. SARS-CoV-2 induces an increase of the LD biogenesis in different human**
505 **pulmonary cell lines.**

506 Human pulmonary cell lines were infected with SARS-CoV-2 at MOI of 0.01 for 48h. (A
507 and C) LDs were captured by fluorescent microscopy after Oil Red O staining (Red) and
508 nuclei stained with DAPI (Blue). (B and D) LDs were evaluated by ImageJ software
509 analysis by the measurement of the fluorescent area. Data are expressed of three
510 independent experiments. *p <0.05 versus uninfected cells. Scale bar 20µm.

511

512

513 **References**

514 Abrantes, J.L., Alves, C.M., Costa, J., Almeida, F.C., Sola-Penna, M., Fontes, C.F., and Souza,
515 T.M. (2012). Herpes simplex type 1 activates glycolysis through engagement of the enzyme 6-
516 phosphofructo-1-kinase (PFK-1). Biochim Biophys Acta *1822*, 1198-1206.
517 Almeida, P.E., Roque, N.R., Magalhaes, K.G., Mattos, K.A., Teixeira, L., Maya-Monteiro, C.,
518 Almeida, C.J., Castro-Faria-Neto, H.C., Ryffel, B., Quesniaux, V.F.*, et al.* (2014). Differential
519 TLR2 downstream signaling regulates lipid metabolism and cytokine production triggered by
520 Mycobacterium bovis BCG infection. Biochim Biophys Acta *1841*, 97-107.
521 Berre, S., Gaudin, R., Cunha de Alencar, B., Desdouits, M., Chabaud, M., Naffakh, N., Rabaza-
522 Gairi, M., Gobert, F.X., Jouve, M., and Benaroch, P. (2013). CD36-specific antibodies block
523 release of HIV-1 from infected primary macrophages and its transmission to T cells. J Exp Med
524 *210*, 2523-2538.
525 Boulant, S., Targett-Adams, P., and McLauchlan, J. (2007). Disrupting the association of hepatitis
526 C virus core protein with lipid droplets correlates with a loss in production of infectious virus. J
527 Gen Virol *88*, 2204-2213.
528 Bozza, P.T., Bakker-Abreu, I., Navarro-Xavier, R.A., and Bandeira-Melo, C. (2011). Lipid body
529 function in eicosanoid synthesis: an update. Prostaglandins Leukot Essent Fatty Acids *85*, 205-
530 213.
531 Bozza, P.T., and Viola, J.P. (2010). Lipid droplets in inflammation and cancer. Prostaglandins
532 Leukot Essent Fatty Acids *82*, 243-250.
533 Camus, G., Herker, E., Modi, A.A., Haas, J.T., Ramage, H.R., Farese, R.V., and Ott, M. (2013).
534 Diacylglycerol acyltransferase-1 localizes hepatitis C virus NS5A protein to lipid droplets and
535 enhances NS5A interaction with the viral capsid core. J Biol Chem *288*, 9915-9923.
536 Carvalho, F.A., Carneiro, F.A., Martins, I.C., Assuncao-Miranda, I., Faustino, A.F., Pereira,
537 R.M., Bozza, P.T., Castanho, M.A., Mohana-Borges, R., Da Poian, A.T.*, et al.* (2012). Dengue
538 virus capsid protein binding to hepatic lipid droplets (LD) is potassium ion dependent and is
539 mediated by LD surface proteins. J Virol *86*, 2096-2108.
540 CDC (2020). Centers for Disease Control and Prevention, Coronavirus Disease 2019 (COVID-
541 19) (https://www.cdc.gov/coronavirus/2019-ncov/lab/rt-pcr-panel-primerprobes.html).
542 Chazal, N., and Gerlier, D. (2003). Virus entry, assembly, budding, and membrane rafts.
543 Microbiol Mol Biol Rev *67*, 226-237, table of contents.
544 Cheng, J.J., Li, J.R., Huang, M.H., Ma, L.L., Wu, Z.Y., Jiang, C.C., Li, W.J., Li, Y.H., Han, Y.X.,
545 Li, H.*, et al.* (2016). CD36 is a co-receptor for hepatitis C virus E1 protein attachment. Sci Rep
546 *6*, 21808.
547 Cheung, W., Gill, M., Esposito, A., Kaminski, C.F., Courousse, N., Chwetzoff, S., Trugnan, G.,
548 Keshavan, N., Lever, A., and Desselberger, U. (2010). Rotaviruses associate with cellular lipid
549 droplet components to replicate in viroplasms, and compounds disrupting or blocking lipid
550 droplets inhibit viroplasm formation and viral replication. J Virol *84*, 6782-6798.
551 Chitraju, C., Mejhert, N., Haas, J.T., Diaz-Ramirez, L.G., Grueter, C.A., Imbriglio, J.E., Pinto,
552 S., Koliwad, S.K., Walther, T.C., and Farese, R.V. (2017). Triglyceride Synthesis by DGAT1
553 Protects Adipocytes from Lipid-Induced ER Stress during Lipolysis. Cell Metab *26*, 407-
554 418.e403.
555 Codo, A.C., Davanzo, G.G., Monteiro, L.B., de Souza, G.F., Muraro, S.P., Virgilio-da-Silva, J.V.,
556 Prodonoff, J.S., Carregari, V.C., de Biagi Junior, C.A.O., Crunfli, F.*, et al.* (2020). Elevated
557 Glucose Levels Favor SARS-CoV-2 Infection and Monocyte Response through a HIF-
558 1α/Glycolysis-Dependent Axis. Cell Metab.
559 Coffey, C.M., Sheh, A., Kim, I.S., Chandran, K., Nibert, M.L., and Parker, J.S. (2006). Reovirus
560 outer capsid protein micro1 induces apoptosis and associates with lipid droplets, endoplasmic
561 reticulum, and mitochondria. J Virol *80*, 8422-8438.

562 Coperchini, F., Chiovato, L., Croce, L., Magri, F., and Rotondi, M. (2020). The cytokine storm
563 in COVID-19: An overview of the involvement of the chemokine/chemokine-receptor system.
564 Cytokine Growth Factor Rev *53*, 25-32.
565 Febbraio, M., Hajjar, D.P., and Silverstein, R.L. (2001). CD36: a class B scavenger receptor
566 involved in angiogenesis, atherosclerosis, inflammation, and lipid metabolism. J Clin Invest *108*,
567 785-791.
568 Filipe, A., and McLauchlan, J. (2015). Hepatitis C virus and lipid droplets: finding a niche. Trends
569 Mol Med *21*, 34-42.
570 Fintelman-Rodrigues, N., Sacramento, C.Q., Lima, C.R., da Silva, F.S., Ferreira, A.C., Mattos,
571 M., de Freitas, C.S., Soares, V.C., Gomes Dias, S.d.S., Temerozo, J.R.*, et al.* (2020). Atazanavir
572 inhibits SARS-CoV-2 replication and pro-inflammatory cytokine production. bioRxiv,
573 2020.2004.2004.020925.
574 Gao, R., Bhatnagar, J., Blau, D.M., Greer, P., Rollin, D.C., Denison, A.M., Deleon-Carnes, M.,
575 Shieh, W.J., Sambhara, S., Tumpey, T.M.*, et al.* (2013). Cytokine and chemokine profiles in lung
576 tissues from fatal cases of 2009 pandemic influenza A (H1N1): role of the host immune response
577 in pathogenesis. Am J Pathol *183*, 1258-1268.
578 Herker, E., Harris, C., Hernandez, C., Carpentier, A., Kaehlcke, K., Rosenberg, A.R., Farese,
579 R.V., and Ott, M. (2010). Efficient hepatitis C virus particle formation requires diacylglycerol
580 acyltransferase-1. Nat Med *16*, 1295-1298.
581 Herker, E., and Ott, M. (2012). Emerging role of lipid droplets in host/pathogen interactions. J
582 Biol Chem *287*, 2280-2287.
583 Laufman, O., Perrino, J., and Andino, R. (2019). Viral Generated Inter-Organelle Contacts
584 Redirect Lipid Flux for Genome Replication. Cell *178*, 275-289.e216.
585 Lee, J.Y., Cortese, M., Haselmann, U., Tabata, K., Romero-Brey, I., Funaya, C., Schieber, N.L.,
586 Qiang, Y., Bartenschlager, M., Kallis, S.*, et al.* (2019). Spatiotemporal Coupling of the Hepatitis
587 C Virus Replication Cycle by Creating a Lipid Droplet- Proximal Membranous Replication
588 Compartment. Cell Rep *27*, 3602-3617.e3605.
589 Lu, R., Zhao, X., Li, J., Niu, P., Yang, B., Wu, H., Wang, W., Song, H., Huang, B., Zhu, N.*, et*
590 *al.* (2020). Genomic characterisation and epidemiology of 2019 novel coronavirus: implications
591 for virus origins and receptor binding. Lancet *395*, 565-574.
592 Lyn, R.K., Hope, G., Sherratt, A.R., McLauchlan, J., and Pezacki, J.P. (2013). Bidirectional lipid
593 droplet velocities are controlled by differential binding strengths of HCV core DII protein. PLoS
594 One *8*, e78065.
595 Martín-Acebes, M.A., Blázquez, A.B., Jiménez de Oya, N., Escribano-Romero, E., and Saiz, J.C.
596 (2011). West Nile virus replication requires fatty acid synthesis but is independent on
597 phosphatidylinositol-4-phosphate lipids. PLoS One *6*, e24970.
598 Meroni, L., Giacomet, V., Morelli, P., Erba, P., Galazzi, M., Riva, A., Viganò, A., and Galli, M.
599 (2005). Increased CD36 expression in vertically human immunodeficiency virus-infected
600 children unrelated to antiretroviral therapy. Pediatr Infect Dis J *24*, 576-577.
601 Miyanari, Y., Atsuzawa, K., Usuda, N., Watashi, K., Hishiki, T., Zayas, M., Bartenschlager, R.,
602 Wakita, T., Hijikata, M., and Shimotohno, K. (2007). The lipid droplet is an important organelle
603 for hepatitis C virus production. Nat Cell Biol *9*, 1089-1097.
604 Novoa, R.R., Calderita, G., Arranz, R., Fontana, J., Granzow, H., and Risco, C. (2005). Virus
605 factories: associations of cell organelles for viral replication and morphogenesis. Biol Cell *97*,
606 147-172.
607 Pereira-Dutra, F.S., Teixeira, L., de Souza Costa, M.F., and Bozza, P.T. (2019). Fat, fight, and
608 beyond: The multiple roles of lipid droplets in infections and inflammation. J Leukoc Biol *106*,
609 563-580.
610 Peschke, T., Bender, A., Nain, M., and Gemsa, D. (1993). Role of macrophage cytokines in
611 influenza A virus infections. Immunobiology *189*, 340-355.
612 Samsa, M.M., Mondotte, J.A., Iglesias, N.G., Assuncao-Miranda, I., Barbosa-Lima, G., Da Poian,
613 A.T., Bozza, P.T., and Gamarnik, A.V. (2009). Dengue virus capsid protein usurps lipid droplets
614 for viral particle formation. PLoS Pathog *5*, e1000632.

Schönborn, J., Oberstrass, J., Breyel, E., Tittgen, J., Schumacher, J., and Lukacs, N. (1991). Monoclonal antibodies to double-stranded RNA as probes of RNA structure in crude nucleic acid extracts. Nucleic Acids Res *19*, 2993-3000.

Shen, B., Yi, X., Sun, Y., Bi, X., Du, J., Zhang, C., Quan, S., Zhang, F., Sun, R., Qian, L.*, et al.* (2020). Proteomic and Metabolomic Characterization of COVID-19 Patient Sera. Cell *182*, 59-72.e15.

Souza-Moreira, L., Soares, V.C., Dias, S.D.S.G., and Bozza, P.T. (2019). Adipose-derived Mesenchymal Stromal Cells Modulate Lipid Metabolism and Lipid Droplet Biogenesis via AKT/mTOR -PPARγ Signalling in Macrophages. Sci Rep *9*, 20304.

Syed, G.H., Amako, Y., and Siddiqui, A. (2010). Hepatitis C virus hijacks host lipid metabolism. Trends Endocrinol Metab *21*, 33-40.

Takahashi, T., and Suzuki, T. (2011). Function of membrane rafts in viral lifecycles and host cellular response. Biochem Res Int *2011*, 245090.

Temerozo, J.R., Sacramento, C.Q., Fintelman-Rodrigues, N., Pão, C.R.R., de Freitas, C.S., da Silva Gomes Dias, S., Ferreira, A.C., Mattos, M., Soares, V.C., Teixeira, L.*, et al.* (2020). The neuropeptides VIP and PACAP inhibit SARS-CoV-2 replication in monocytes and lung epithelial cells, decrease the production of proinflammatory cytokines, and VIP levels are associated with survival in severe Covid-19 patients. bioRxiv, 2020.2007.2025.220806.

Viktorova, E.G., Nchoutmboube, J.A., Ford-Siltz, L.A., Iverson, E., and Belov, G.A. (2018). Phospholipid synthesis fueled by lipid droplets drives the structural development of poliovirus replication organelles. PLoS Pathog *14*, e1007280.

Villareal, V.A., Rodgers, M.A., Costello, D.A., and Yang, P.L. (2015). Targeting host lipid synthesis and metabolism to inhibit dengue and hepatitis C viruses. Antiviral Res *124*, 110-121.

Wu, F., Zhao, S., Yu, B., Chen, Y.M., Wang, W., Song, Z.G., Hu, Y., Tao, Z.W., Tian, J.H., Pei, Y.Y.*, et al.* (2020). A new coronavirus associated with human respiratory disease in China. Nature *579*, 265-269.

Yang, W., Hood, B.L., Chadwick, S.L., Liu, S., Watkins, S.C., Luo, G., Conrads, T.P., and Wang, T. (2008). Fatty acid synthase is up-regulated during hepatitis C virus infection and regulates hepatitis C virus entry and production. Hepatology *48*, 1396-1403.

Yuan, S., Chu, H., Chan, J.F., Ye, Z.W., Wen, L., Yan, B., Lai, P.M., Tee, K.M., Huang, J., Chen, D.*, et al.* (2019). SREBP-dependent lipidomic reprogramming as a broad-spectrum antiviral target. Nat Commun *10*, 120.

Zhang, J., Lan, Y., and Sanyal, S. (2017). Modulation of Lipid Droplet Metabolism-A Potential Target for Therapeutic Intervention in. Front Microbiol *8*, 2286.

Zhou, F., Yu, T., Du, R., Fan, G., Liu, Y., Liu, Z., Xiang, J., Wang, Y., Song, B., Gu, X.*, et al.* (2020a). Clinical course and risk factors for mortality of adult inpatients with COVID-19 in Wuhan, China: a retrospective cohort study. Lancet *395*, 1054-1062.

Zhou, P., Yang, X.L., Wang, X.G., Hu, B., Zhang, L., Zhang, W., Si, H.R., Zhu, Y., Li, B., Huang, C.L.*, et al.* (2020b). A pneumonia outbreak associated with a new coronavirus of probable bat origin. Nature *579*, 270-273.

Zhu, N., Zhang, D., Wang, W., Li, X., Yang, B., Song, J., Zhao, X., Huang, B., Shi, W., Lu, R.*, et al.* (2020). A Novel Coronavirus from Patients with Pneumonia in China, 2019. N Engl J Med *382*, 727-733.

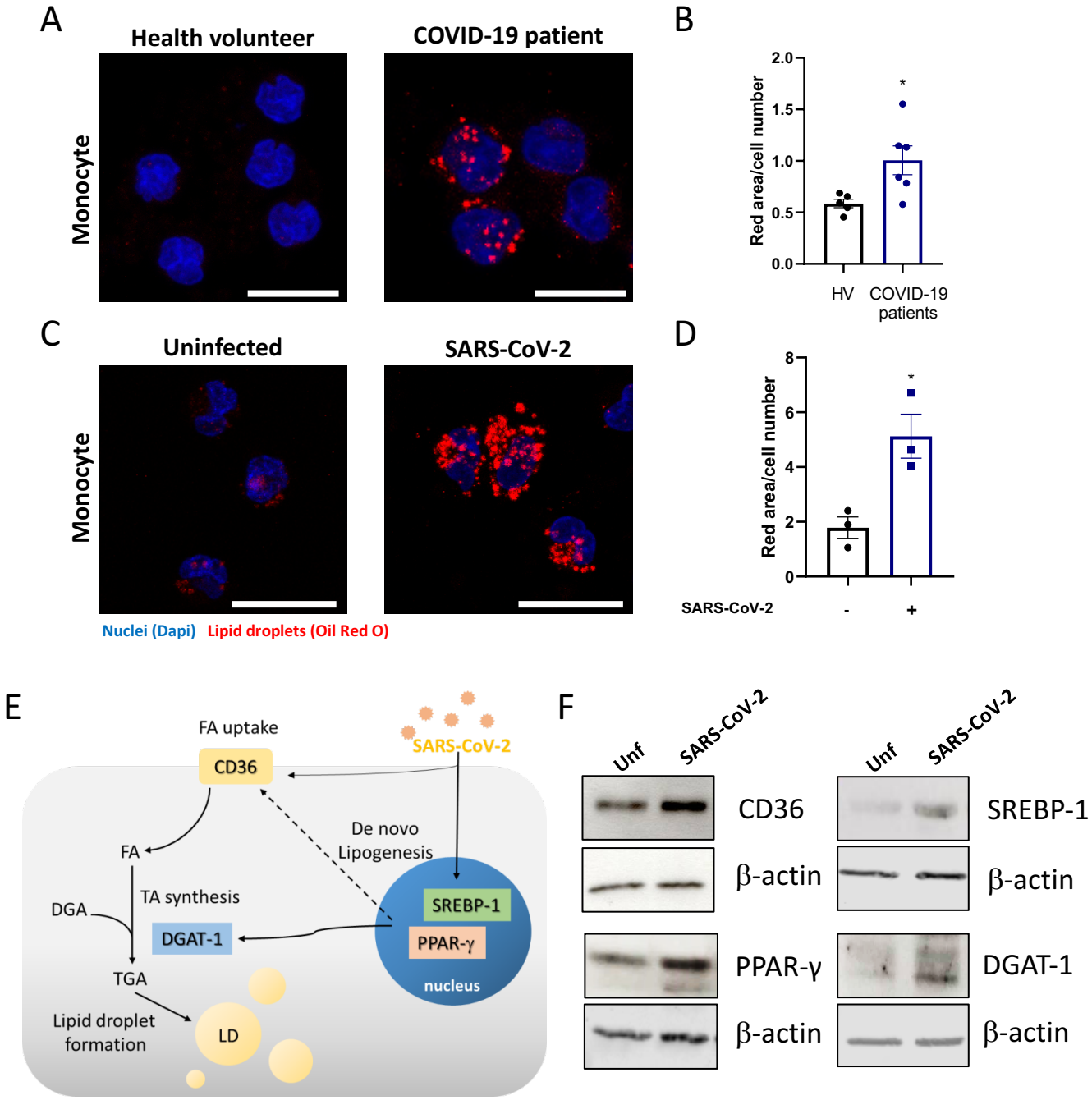
A
Health volunteer
COVID-19 patient
Monocyte
B
Red area/cell number
HV
COVID-19 patients
C
Uninfected
SARS-CoV-2
Monocyte
D
Red area/cell number
SARS-CoV-2
Nuclei (Dapi)
Lipid droplets (Oil Red O)
E
FA uptake
CD36
SARS-CoV-2
De novo Lipogenesis
FA
TA synthesis
DGA
DGAT-1
SREBP-1
PPAR-γ
nucleus
TGA
Lipid droplet formation
LD
F
Unf
SARS-CoV-2
CD36
SREBP-1
β-actin
PPAR-γ
DGAT-1
G
CD36/β-actin
SREBP-1/β-actin
PPAR-γ/β-actin
DGAT-1/β-actin
SARS-CoV-2

Figure 1

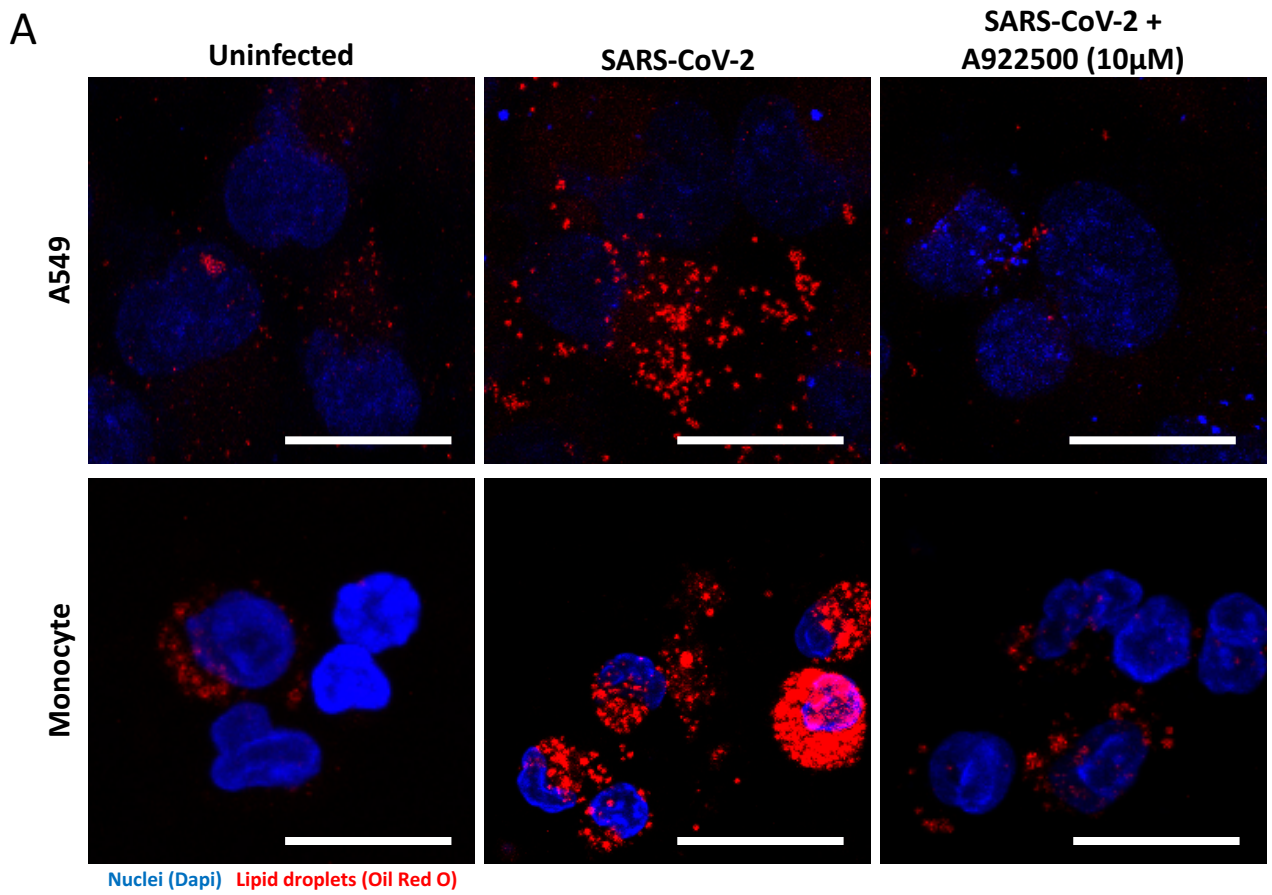
A
Uninfected
SARS-CoV-2
SARS-CoV-2 +
A922500 (10µM)
A549
Monocyte
Nuclei (Dapi)
Lipid droplets (Oil Red O)

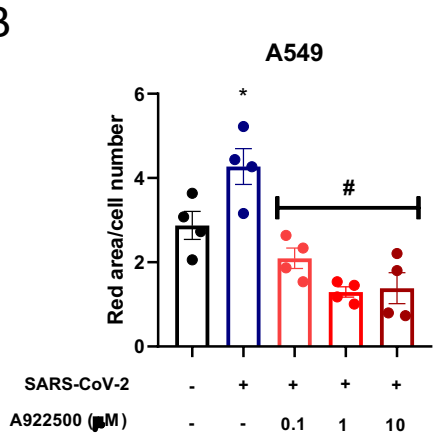
B
A549
Red area/cell number
0
2
4
6
*
#
SARS-CoV-2 - + + + +
A922500 (µM) - - 0.1 1 10

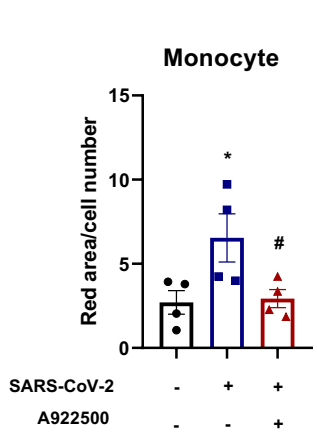
C
Monocyte
Red area/cell number
0
5
10
15
*
#
SARS-CoV-2 - + +
A922500 - - +

Figure 2

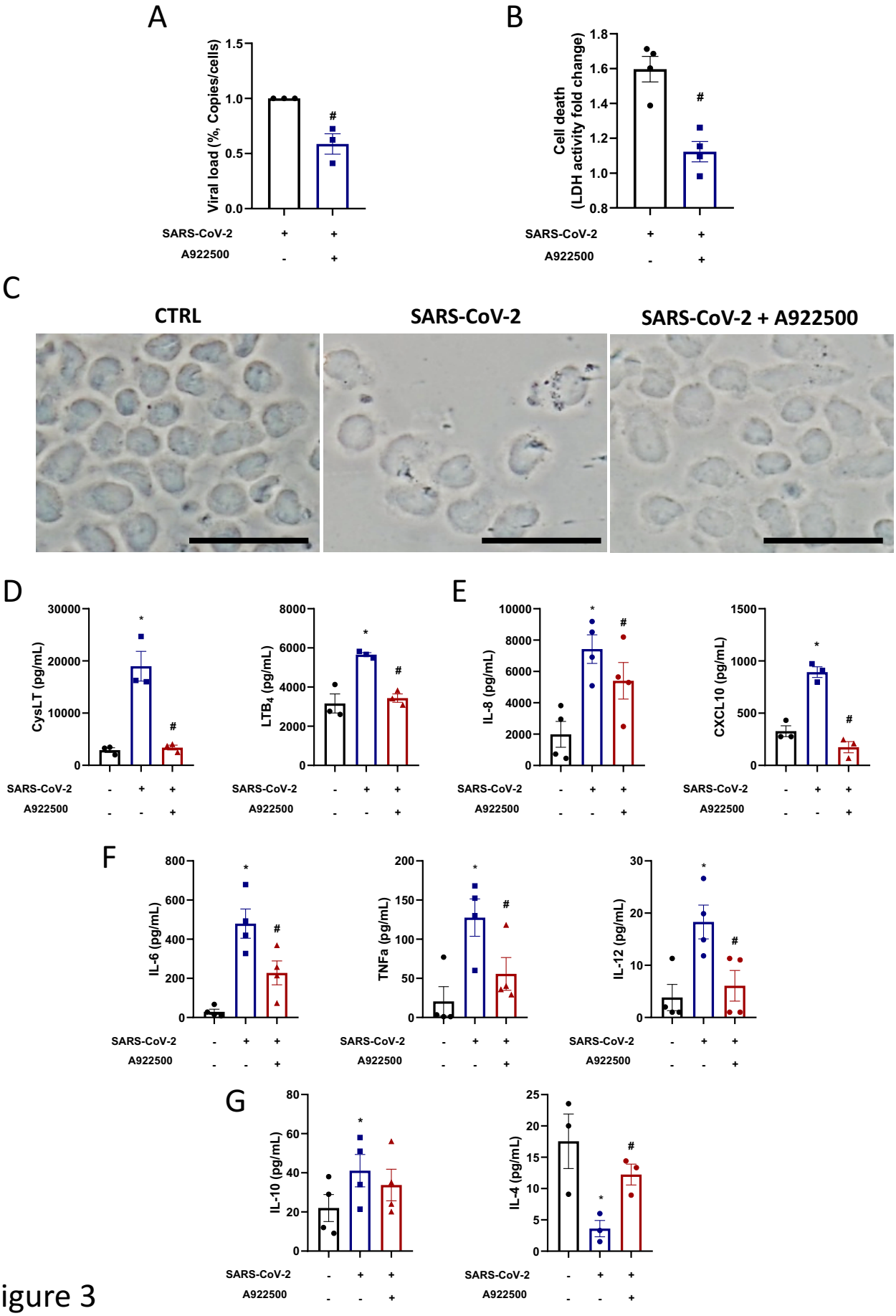
A
Viral load (%, Copies/cells)
1.5
1.0
0.5
0.0
#
SARS-CoV-2 + +
A922500 - +
B
Cell death
(LDH activity fold change)
1.8
1.6
1.4
1.2
1.0
0.8
#
SARS-CoV-2 + +
A922500 - +
C
CTRL
SARS-CoV-2
SARS-CoV-2 + A922500
D
CysLT (pg/mL)
30000
20000
10000
0
LTB4 (pg/mL)
8000
6000
4000
2000
0
SARS-CoV-2 - + +
A922500 - - +
E
IL-8 (pg/mL)
10000
8000
6000
4000
2000
0
CXCL10 (pg/mL)
1500
1000
500
0
SARS-CoV-2 - + +
A922500 - - +
F
IL-6 (pg/mL)
800
600
400
200
0
TNFa (pg/mL)
200
150
100
50
0
IL-12 (pg/mL)
30
20
10
0
SARS-CoV-2 - + +
A922500 - - +
G
IL-10 (pg/mL)
80
60
40
20
0
IL-4 (pg/mL)
25
20
15
10
5
0
SARS-CoV-2 - + +
A922500 - - +

Figure 3

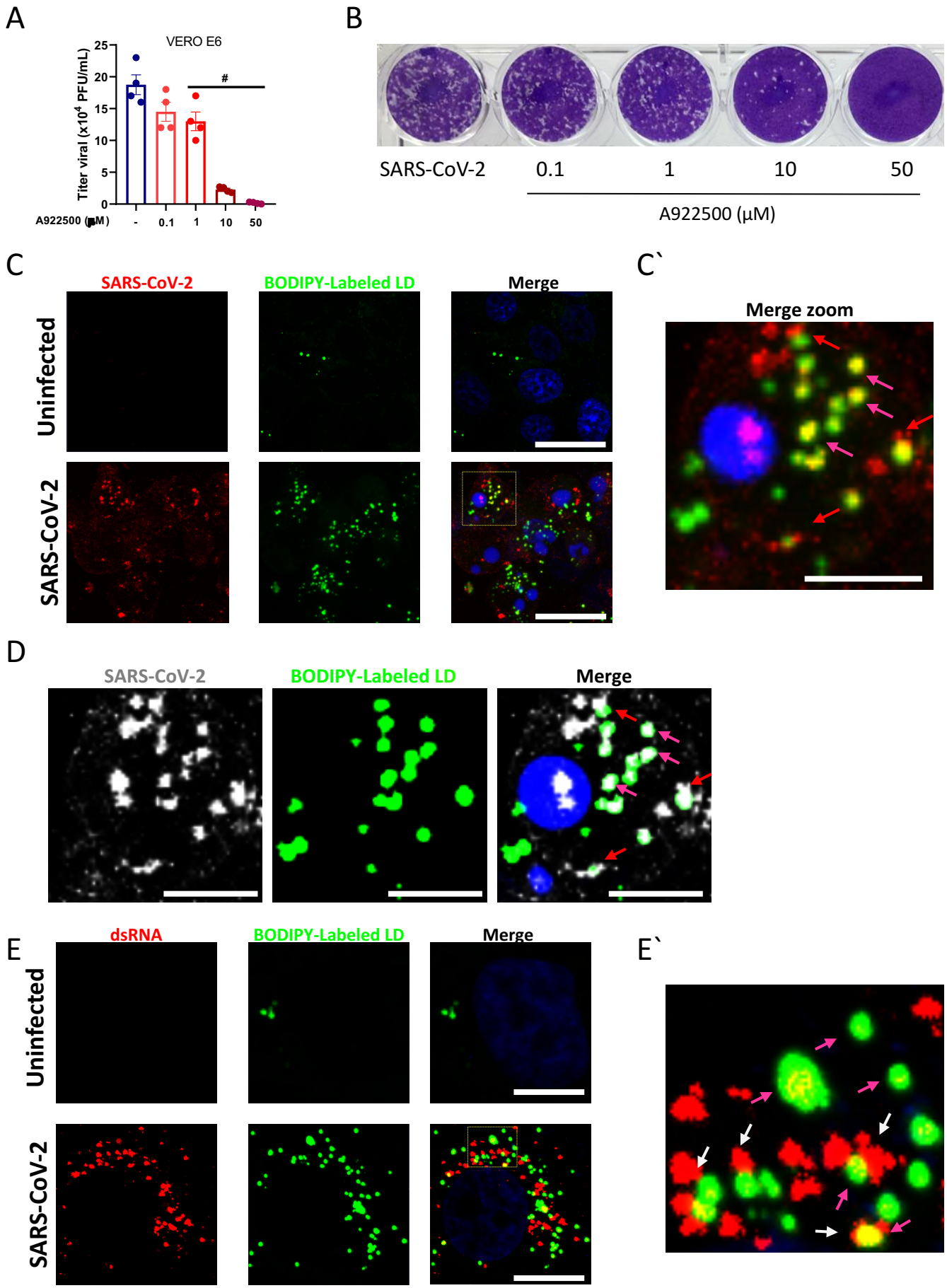
A
VERO E6
Titer viral (x10^4 PFU/mL)
25
20
15
10
5
0
#
A922500 (μM)
-
0.1
1
10
50
B
SARS-CoV-2
0.1
1
10
50
A922500 (μM)
C
SARS-CoV-2
BODIPY-Labeled LD
Merge
Uninfected
SARS-CoV-2
C`
Merge zoom
D
SARS-CoV-2
BODIPY-Labeled LD
Merge
E
dsRNA
BODIPY-Labeled LD
Merge
Uninfected
SARS-CoV-2
E`

Figure 4

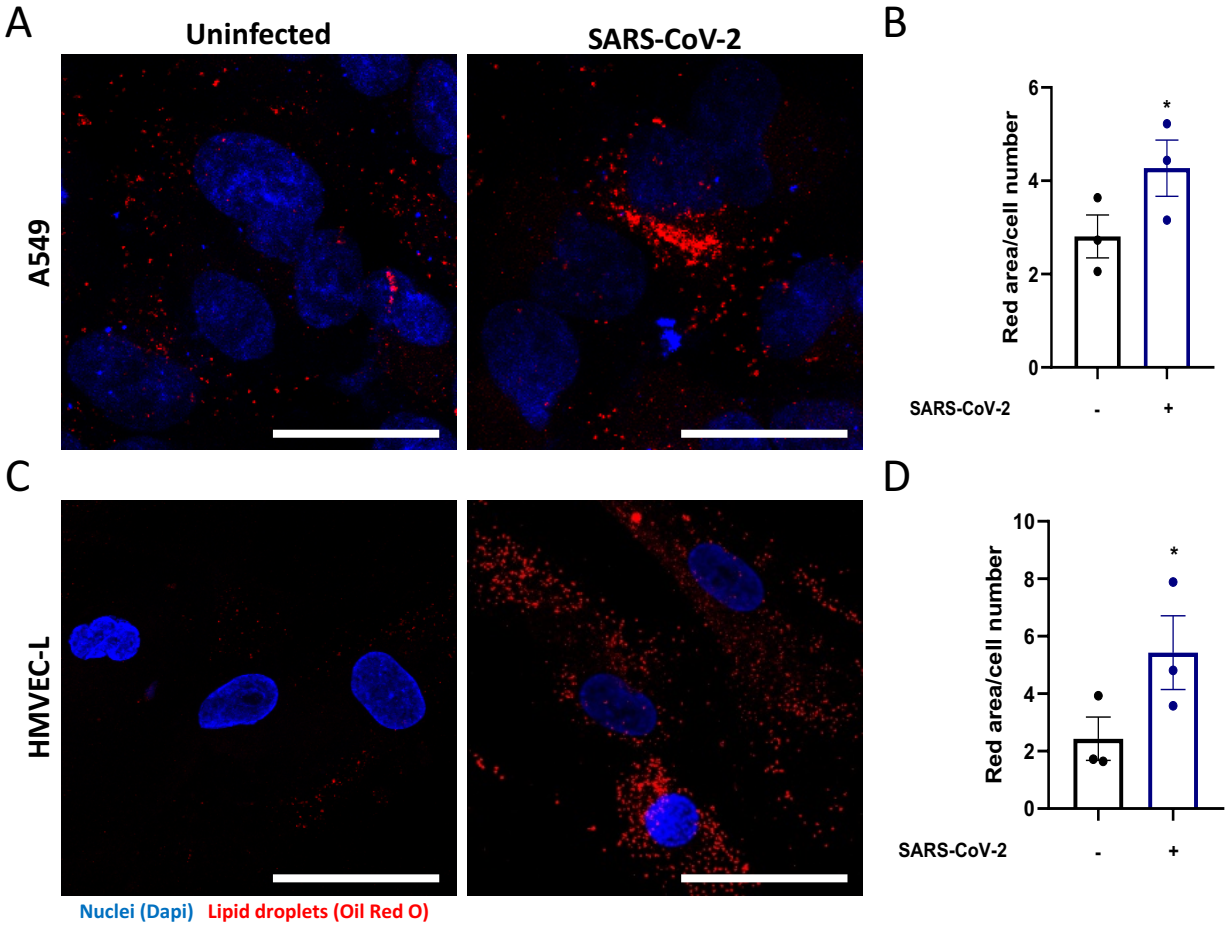

Supplementary Figure 1